Expanding the palette of SWIR emitting nanoparticles based on Au nanoclusters for single-particle tracking microscopy

Apolline A. Simon[1,2,3,+], Lucie Haye[4,+], Abdallah Alhalabi[5], Stéphane Mornet[3], Andreas Reisch[4,6,], Xavier Le Guével[5,*] and Laurent Cognet[1,2,*].*

[1]*Univ. Bordeaux, Laboratoire Photonique Numérique et Nanosciences (LP2N), UMR 5298, F-33400 Talence, France*

[2]*Institut d'Optique & CNRS, LP2N UMR 5298, F-33400 Talence, France*

[3]*Univ. Bordeaux, CNRS, Bordeaux INP, ICMCB, UMR 5026, 33600 Pessac, France*

[4]*Université de Strasbourg, CNRS, Laboratoire de Bioimagerie et Pathologies UMR 7021, F-67000, Strasbourg France*

[5]*University of Grenoble Alpes, Institute for Advanced Biosciences, INSERM1209/CNRS-UMR5309-Grenoble-France*

[6]*Université de Strasbourg, INSERM, Biomaterials and Bioengineering laboratory UMR 1121, F-67000, Strasbourg, France*

[+] equal contribution

E-mail: *laurent.cognet@u-bordeaux.fr; xavier.le-guevel@univ-grenoble-alpes.fr; reisch@unistra.fr*

Keywords: nanoparticle, single particle tracking, SWIR imaging, luminescence, photostability,

Abstract: Single-molecule localization microscopy has proved very promising to unravel the dynamics and molecular architecture of thin biological samples down to the nanoscale. However, achieving meaningful results in complex, thick biological tissues requires shifting the observation wavelengths to the shortwave-infrared (SWIR) region, where biological tissues are most transparent. In consequence, nanomaterials with optical activity in the SWIR exhibiting brightness and photostability suitable for detection at the single-molecule level are needed. Currently mainly single-walled carbon nanotubes (SWCNTs) satisfy this, but are inherently 1D objects. Here we present 0D ultra-small gold nanoclusters (AuNCs, <3nm) and ~25 nm AuNC-loaded-polymeric particles that can be detected at the single-particle level in the SWIR. Thanks to their high brightness and excellent photostability, we show that the dynamics

of the spherical polymeric particles can be followed at the single-particle level in solution at video rates for minutes. Analysis of the mean square displacement confirms the diameter of the particles in aqueous media, and enables us to compare their brightness with that of biocompatible SWCNTs. This extends the library of SWIR emitting nanomaterials to 0D nano-objects of variable size for single-molecule localization microscopy in the second biological window, opening unprecedented possibilities for mapping structure and dynamics of complex biological systems.

Introduction

The development of luminescent nanoprobes emitting in the second transparency biological window, where light penetration is maximized in biological tissue, is the subject of intense research for advanced imaging in biology and medical applications, allowing to observe biological processes in real and complex environments[1–6]. The corresponding wavelength range lies in the shortwave infrared (SWIR) domain (900-1700 nm), where biological autofluorescence and light scattering are minimal[7]. Although the development of currently commercially available cameras based on narrower bandgap semiconductor alloys such as InGaAs and HgCdTe enables fluorescence imaging in the SWIR, a drawback of this long wavelength range concerns the degraded resolution of optical microscopes. A powerful solution to this issue can be provided by localization microscopy approaches that have the capacity to bypass the diffraction limited resolution of optical microscopes. In particular, single particle tracking localization microscopy allows to interrogate molecular dynamics at the nanoscale in a variety of environments including biological specimens such as live cells or biological tissues[8,9]. Yet, applications to biological tissues still rely on a very limited number of SWIR emitting nanoprobes that are bright and photostable enough to be detected through thick samples. Among them, luminescent single walled carbon nanotubes (SWCNTs), have proved extremely valuable for single particle tracking (SPT) applications in tissues[10,11]. In this context, the field would benefit from other SWIR emitting nanoparticles (NPs) having spherical morphologies to complement one-dimensional SWCNT probes which display singular diffusion properties in crowded environments as compared to spherical ones[12]. Developing SWIR NPs having distinct morphologies would indeed be key to control their accessibility in specific areas of biological tissues.

A suitable single particle probe should possess the following properties: high photoluminescence (PL) brightness for super-localization well below the emission wavelength, excellent photostability for long recording and small dimensions for accessing restricted environments.

It was recently shown that atomically precise gold nanoclusters (AuNCs) represent a promising class of SWIR probes[13–15] that bear the advantages to be ultra-small (<3 nm), biocompatible, easy to functionalize, with tunable SWIR PL. Yet their per particle brightness and PL stability remain unknown so the possibility of detecting them at the single particle level has yet to be elucidated. An alternative approach consists in encapsulating AuNCs at high amounts in polymers to form 0D nanoparticles[16–18] (AuPolyNPs). Here we demonstrate that anisotropic surface charged AuNCs can be detected at the single particle level on 2D surfaces, and AuPolyNPs can be detected and tracked in aqueous environments akin SWIR emitting SWCNTs, thus constituting a novel alternative for localization microscopy applications in the SWIR domain (**Figure 1**).

Results and discussion

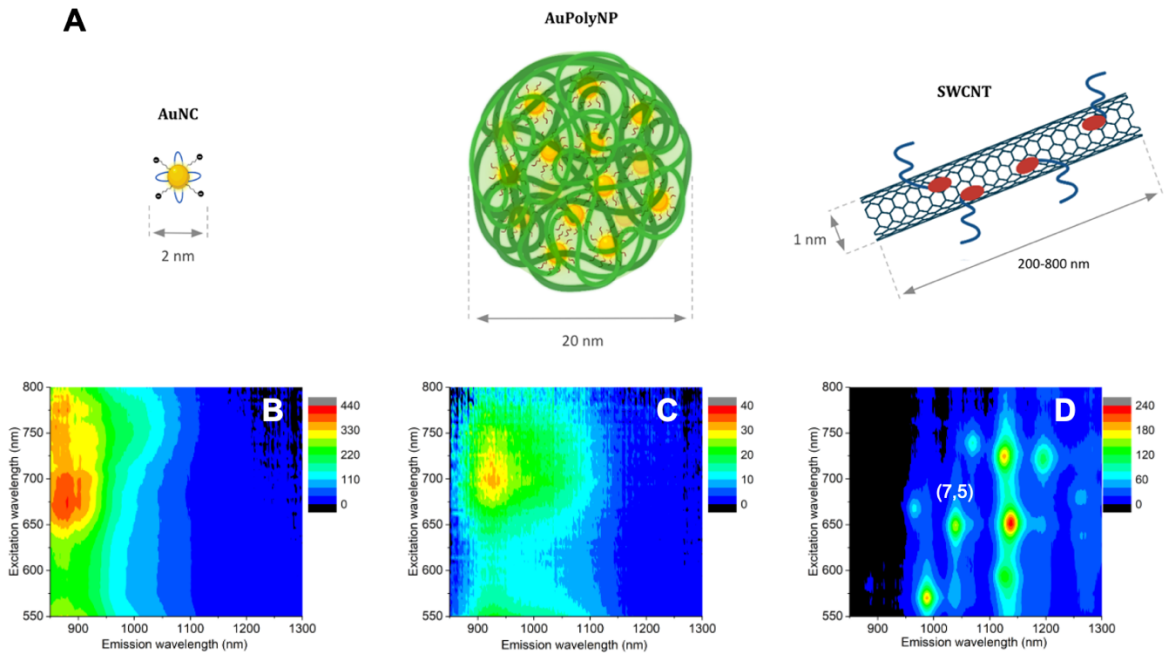

Figure 1. *A) Scheme of the different SWIR emitters. 2D PL maps of AuNCs (B), AuPolyNPs (C) and SWCNTs (D). The peak corresponding to the (7,5) chirality is indicated.*

Water soluble ultra-small AuNCs surfaced-functionalized with short dithiol-terminated poly(ethylene glycol) molecules were chosen for their broad absorption (**Figure S1**), high PL with QY reaching 6.5% previously identified at the ensemble level (**Table S1**). AuNCs were prepared as previously described[14,19,20]: in short, they were synthesized by a bottom-up approach using tetrachloroauric(III) acid trihydrate ($HAuCl_4 \cdot 3H_2O$) and a 3.5/0.5 molar ratio of monodentate mercaptohexanoic acid (MHA) and the bidentate ligand hexa (ethylene glycol) dithiol (HDT) in alkaline solution. This generated AuNCs having core sizes below 3 nm (according to high-resolution TEM, **Figure S2**) and displaying a broad absorption range from visible to near-infrared and corresponding emission in the SWIR from 800 to 1200 nm (**Figure 1**).

AuNC loaded polymer NPs (AuPolyNPs) were prepared through nanoprecipitation.[21,22] For this, AuNCs stabilized by the hydrophobic ligand dodecanethiol (DDT) (**SI** and **Figure S3, S4**) were used to make them soluble in organic solutions and insoluble in aqueous ones, which is required for efficient encapsulation upon nanoprecipitation[16,23,24]. Here, we focused on AuPolyNPs with a small size, below 30 nm, which are more suitable for single particle tracking applications in complex environments. In consequence, a poly(ethyl methacrylate) (PEMA) polymer bearing 10 mol% of methacrylic acid groups, known to reduce particle size, was chosen with an intermediate loading of AuNCs[16,25] (17 wt% relative to the total mass of polymer and AuNCs). DLS results gave a mean hydrodynamic particle size of 27 ± 2 nm. TEM micrographs showed a narrow monomodal size distribution with a mean size of 18 ± 3 nm, which is in reasonable agreement with DLS, considering that TEM gives the hard-core size of dried NPs (**Figure S5**). AuPolyNP optical spectra demonstrate that the optical properties of AuNCs are mostly retained when encapsulated in polymer NPs (**Figure 1C** and **Figure S3**). The resulting AuPolyNPs displayed a broad absorption from < 400 to 1000 nm, with bands characteristic of the encapsulated AuNCs, notably at 415 nm and 705 nm. They emitted in the SWIR from 900 to 1200 nm, with a PL QY of 0.65 %.

For comparison, we also prepared SWCNTs solutions by encapsulating raw SWCNT material in phospholipid-PEG (18:0 PEG5000 DSPE, Laysan Bio), a well-known suspending agent for biological applications[26,27]. We chose SWCNTs synthesized by the HiPCo method (Batch 195.7, Rice University) containing high amount of the semi-conducting (7,5) nanotube chirality[28] with the objective of using identical excitation wavelengths and intensities for AuNCs, AuPolyNPs and SWCNTs to enable direct brightness comparisons. Indeed, (7,5) SWCNTs display strong absorption at 660 nm while emitting at ~1025 nm, and are commonly

applied in biological applications upon excitation at 660 nm[26]. This makes them a fair standard for the Au-based objects investigated in this work. We bear in mind that each type of nano-objects displays different absorption spectra and are therefore not strictly optimally excited at the same excitation wavelengths, yet the choice of a common excitation wavelength at 660 nm is a good compromise since AuNC-based emitters display broad absorption spectra around this wavelength.

The optical properties of AuNCs, AuPolyNPs and SWCNTs were inspected at the single particle level using a single molecule fluorescence microscope optimized for SWIR imaging. **Figure 2** shows typical images of AuNCs, AuPolyNPs and SWCNTs dispersed on a glass-slide and recorded with 30 ms integration time at identical excitation laser intensities.

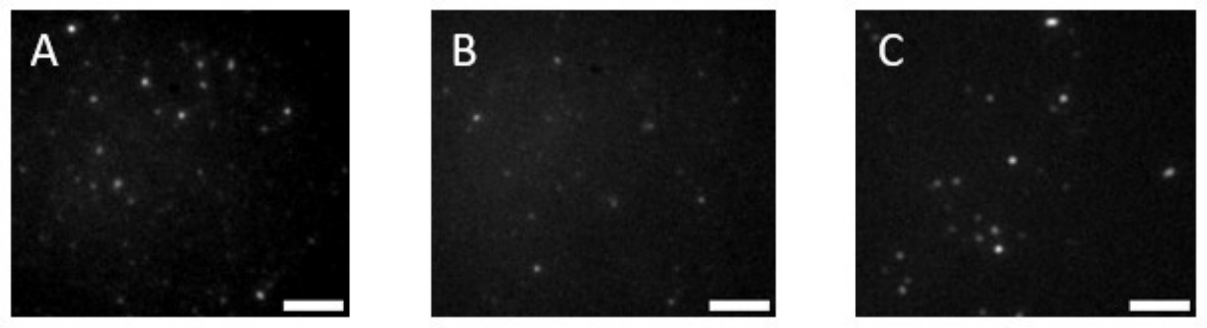

Figure 2. *Fluorescence images of individual AuNCs (A), AuPolyNPs (B), SWCNTs (C) immobilized on coverslips excited at 660 nm (700 W/cm^2). AuNCs were detected in dried state while AuNPs and SWCNTs were detected in aqueous environments. Scale bar: 5 µm*

We found that AuNCs could be detected as individualized entities when dried on the polylysine-coated coverslips (but not in aqueous conditions, not shown), while AuPolyNPs and SWCNTs are easily detected both in dried and aqueous environments. Indeed, from images displayed in **Figure 2**, the detection of diffraction limited points (having Full Width at Half Maximum close to the diffraction limit given by 0,61λ/NA ~ 480 nm) is a first indication that AuNCs and AuPolyNPs are detected at the single particle level. Note the presence of few elongated particles in **Figure 2C** as expected for SWCNTs with longer lengths than the diffraction limit. In order to confirm that the great majority of resolved discrete spots may be attributed to single NPs, we constructed the histograms of signal intensities corresponding to each spot by fitting the diffraction limited signals to 2D Gaussian curves having width equal to the microscope diffraction limit (see Experimental Methods, **Figure 3**).

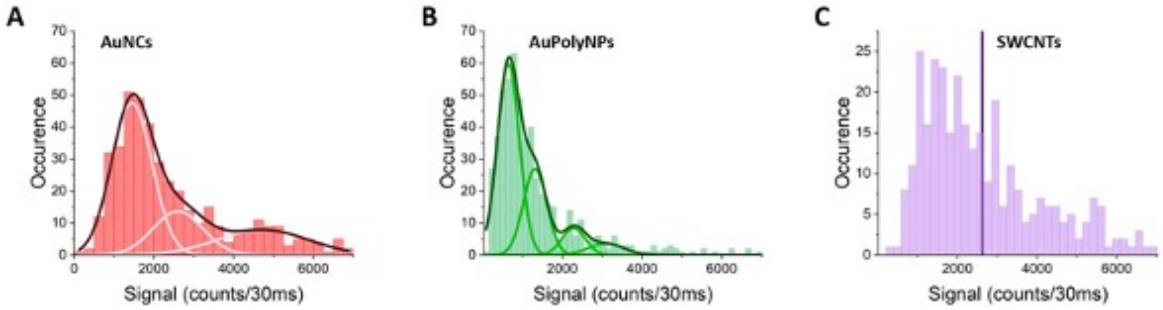

Figure 3: *Evidence for single NP detection. Histogram of the signals for the 3 different samples, AuNCs (dried), AuPolyNPs (aqueous), SWCNTs (aqueous). The distributions in A and B are well fitted by multiple Gaussian curves. The position of the second, third and fourth maxima were multiple of that of the first one. This observation indicates that single particles are detected in the first peak and two and more particles are detected in the others. The histogram in C is broader with median equal to 2700, reflecting a polydisperse distribution as expected for SWCNTs of several lengths*.

The signal intensity histograms reveal the presence of one main population and minority subpopulations having signals that are multiple of the main population one (**Figure 3A-B**). This indicates that single particles correspond to the first populations while the subpopulations represent the situation of two or more particles detected within the diffraction limited spot. Note that for SWCNTs, the signal distribution is less monodisperse as expected by the dispersion of length of nanotube preparations (spanning typically from 200 nm up to 800 nm).

By comparing the PL of the different types of emitters in aqueous environment, AuNCs could not be observed at the single particle level (which was expected from the per particle brightness determined in ensemble, see **Table S1**), yet we observed that it becomes possible to detect them at the single particle level in dried condition with PL levels of the order of that of SWCNTs. We believe this is related to previous observations having shown significant PL enhancement by surface charge injection[20,29]. On the other hand, AuPolyNP emission of single particles (~ 650 counts/30ms) is found to be only ~4 times lower than that of SWCNTs (median ~2700 counts/30ms) that are known to be very bright emitters, bearing in mind that AuPolyNPs and SWCNTs are also very differently shaped objects. Indeed, AuPolyNPs are small spherical NPs (~20-30 nm) in contrast to SWCNTs that are thin and long 1D objects (typically, 400 nm length, 1-3 nm diameter).

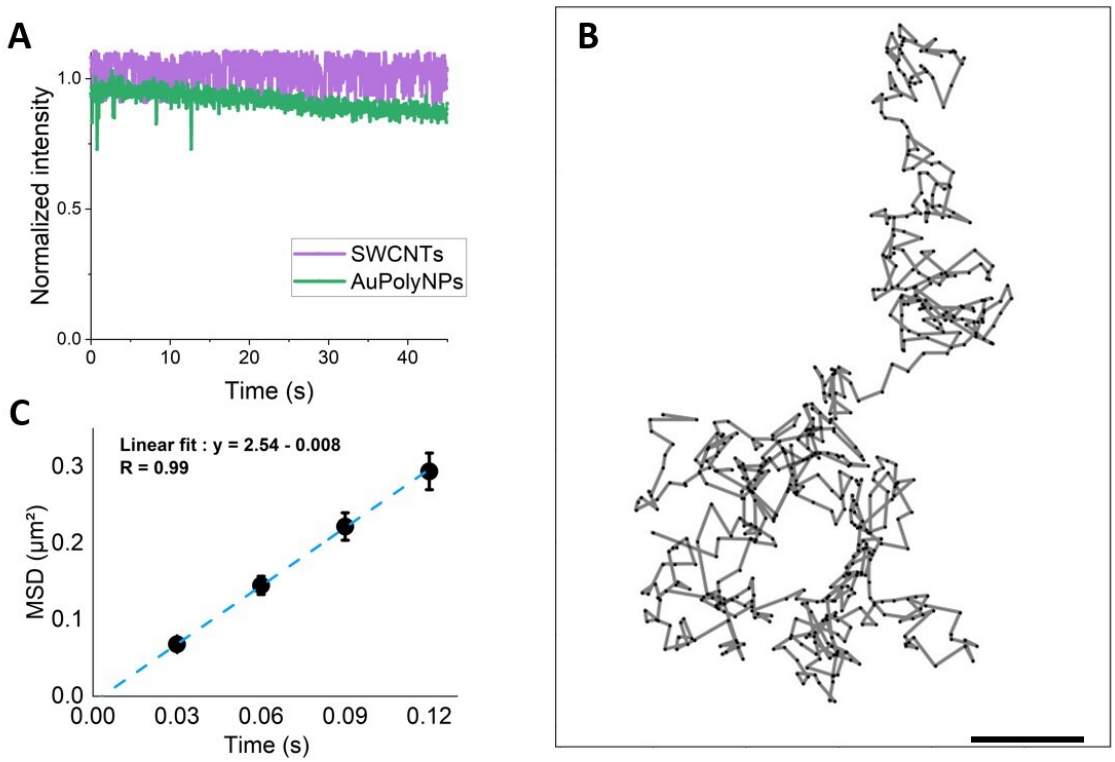

Figure 4. *(A) Photostability of a single AuPolyNC and a single SWCNT (normalized emission intensity). (B) example trajectory of a single AuPolyNC recorded by SPT. Scale bar = 1µm. (C) average MSD plot of 191 trajectories with a linear fit.*

We next investigated the possibility of tracking single AuPolyNPs akin SWCNTs, which have already demonstrated great promise in biological studies due to their SWIR emission range[30,31]. **Figure 4A** shows that single AuPolyNPs immobilized as in **Figure 2A** can be continuously detected at high imaging rate (30 ms integration time) during tens of seconds with low photobleaching. This excellent photostability constitutes a key prerequisite for realistic SPT applications. We next imaged, localized and tracked single AuPolyNPs freely diffusing in a water/glycerol (1:2 vol/vol) solution (see **Movie in SI**). We could record and reconstruct the trajectories of individual AuPolyNPs while they were captured in the depth-of-focus range of the microscope (**Figure 4B**) and analyze their diffusion characteristics. For this, we calculated the average mean square displacement (MSD) of 191 AuPolyNPs trajectories (**Figure 4C**). The MSD is found to be linear as expected for Brownian diffusion. Interestingly, knowledge of the viscosity of the medium ($0.026 \pm 0.002\ Pa.s$)[32,33] allowed us to determine the diffusion constant of the particles and thus retrieve their hydrodynamic diameter from the slope of the MSD using the Stokes-Enstein equation and taking into account localization precision of this experiment (see Experimental Methods). We found a value of $26 \pm 3\ nm$. This average

hydrodynamic diameter measured with a single molecule approach is in excellent agreement with the diameter of $27 \pm 2\ nm$ measured by DLS at the ensemble level.

Interestingly, we were finally able to evaluate the per particle brightness of AuPolyNPs upon excitation at 660 m and compare it with that of SWCNTs owing to the determination of the size of AuPolyNPs obtained by our SPT analysis presented above, and to the knowledge of their molar extinction and quantum yield (**Table S1**). We found 14,000 $M^{-1}.cm^{-1}$ for AuPolyNPs to be compared to 130,000 $M^{-1}.cm^{-1}$ for (7,5) SWCNTs (**Table S1**). This represents a brightness ratio of ~9 in fair agreement with that obtained from our single-particle study (~4 fold) shown in **Figure 3** given the uncertainties on the molar extinction and quantum yield data in ensemble measurements (see **SI**).

Conclusion

This work demonstrates that AuNC-based SWIR emitters constitute a promising route for expanding the palette of fluorescent nanostructures for single particle tracking. Immobilized single water-soluble AuNCs could be easily detected on the single particle level, while polymer NPs encapsulating large amounts of hydrophobic AuNCs (AuPolyNPs) could be tracked over extended periods in solution. Compared with the well-known SWCNTs as bright SWIR emitters, these Au-based SWIR nanostructures can exhibit comparable brightness and emission range under identical excitation conditions. This makes them particularly interesting to complement SWCNTs as diffusion probes in SPT applications to explore and reveal complex and tortuous biological structures (e.g. brain or liver tissue), as they feature very different shapes (0D vs. 1D), which should enable them to access different environments. We also anticipate that advances in the design and synthesis of AuNCs and AuPolyNPs will further enhance their respective optical properties to broaden the range of applications for single-molecule localization microscopy in the SWIR. In particular, loading of AuNCs in polymer NPs offers the possibility to tune the size of the NPs through the choice of the polymer and the assembly conditions over a wide range. At the same time, increasing the loading with AuNCs and further developments in the design of the AuNCs should allow further optimizing their brightness for precise single-particle tracking applications deep inside complex biological tissues. More generally, this study should contribute to the development of novel contrast agents for biological and medical imaging. We further believe that it will also stimulate the development of different formulations used in nanomedicine (biocompatible polymer nanoparticles, liposomes, solid lipid nanoparticles, etc.) loaded with high amounts of SWIR

emitting AuNCs to enhance their optical properties and to monitor their access and fate in biological tissues.

Experimental Methods

AuPolyNPs preparation: Polyethylmethacrylate (PEMA) bearing 10 mol% of methacrylic acid was synthesized through free radical polymerization as described previously[16]. Stock solutions of PEMA were prepared at a concentration of 10 g.L-1 in acetonitrile. These solutions were diluted to 2 $g.L^{-1}$ in acetonitrile, with 17 wt% of AuNCs (relative to the total mass of polymer and AuNC). These solutions were quickly added to a 9-fold volume excess of phosphate buffer (20 mM, pH 7.4) under shaking (Thermomixer comfort, Eppendorf, 1050 rpm at 21°C), followed by further dilution to the desired concentration.

Microscopy setup: The single-molecule fluorescence microscope operating in the SWIR domain was built around a conventional widefield microscope equipped with a 60x/1.27NA Water immersion objective (Nikon) having high transmission in the SWIR. The sample was illuminated at 660 nm (Obis laser, Coherent) at 0.7 kW/cm^2 by reflecting the laser on a 900 nm long pass dichroic mirror (FF875-Di01, Semrock). For AuNCs and AuNPs a 900 nm long pass emission filter (ET900LP, Chroma) was inserted in front of a low-noise SWIR InGaAs camera (Ninox 2, Raptor Photonics) to record single particle images. For SWCNTs, the combination of a 1000 nm long pass filter and a 1050 nm short pass filter (Edmund Optics) allowed to select resonantly excited (7,5) SWCNTs among the other SWCNT chiralities present of the HiPCo sample (see **Figure 1D**).

Sample preparation of immobilized particles: AuNCs, AuPolyNPs or SWCNTs we immobilized them on a glass coverslip functionalized with polylysine (PLL). More precisely, a drop of PLL (0.01wt% in DI water) was placed on a coverslip at room temperature, after rinsing and let to dry for 1 hour. The dispersion of NPs was then placed on the cover slip for another hour, followed by several rinsing. The coverslip was then mounted on the microscope for optical studies.

Single particle brightness analysis: For each NP type, 40 fields of view were acquired with identical excitation laser intensity at 660 nm on the same optical setup (except for the

combination of filters, see above). Each field of view contained optically resolved emission spots as exemplified on **Figure 2.** For analysis, we first used Fidji to rescale the image pixel sizes to 237 nm (in the object plane). All images, we then analyzed with a home-made matlab program where each diffraction limited spot was adjusted by a 2D Gaussian fit which provided the brightness of the spots displayed in **Figure 3** defined as the integrated signal under the 2D Gaussian fits.

Particle size determination via diffusion analysis: AuPolyNPs or SWCNTs were added in a 2:1 v/v glycerol-water mixture. A drop of this solution was sandwiched between two coverslips and sealed by vacuum grease before placing them onto the fluorescence microscope. Movies of diffusing particles were then acquired with a 30 ms exposure time (t_E). Single particle tracking analysis was performed using python homemade codes (Lee, 2020). From the reconstructed trajectories, the Mean Square Displacement (MSD) was then computed, and the diffusion coefficients of each trajectory (D) were extracted using the following formulae: $MSD(t) = \varepsilon - \frac{4}{3}Dt_E + 4Dt$, where ε is related to the localization uncertainty for a static particle (σ) by[34] $\varepsilon = \sigma^2$. **Figure 3C** displays the average MSD obtained from 191 trajectories. Fitting experimental data with a linear curve provided $D = 0.63\ \mu m^2/s$. The offset of the fit contains two terms: static localization uncertainty and a diffusion term during the acquisition of an image. Knowledge of D allowed to determine the static localization and we found $\sigma = 61\ nm$. From the value of the diffusion constant D, the hydrodynamic particle radius (r) could be calculated with the Stokes-Einstein relation $D = \frac{k_B T}{6\pi\eta r}$, where k_B is the Boltzmann coefficient, T the temperature and η the dynamic viscosity of the mixture (Pa.s)

Supporting Information

Supporting Information is available.

Acknowledgements

This work was performed with financial support from CNRS, the University of Bordeaux, the France-BioImaging National Infrastructure (ANR-10-INBS-04-01), the Idex Bordeaux (Grand Research Program GPR LIGHT) and the EUR Light S&T (PIA3 Program, ANR-17-EURE-0027) to L.C; LH, XLG, and AR thank the French Agence Nationale de la Recherche (project LAPIN – ANR-20-CE09-0021-04). XLG thanks France Life Imaging (ANR-11-INBS-0006) for their financial support.

References

[1] C. Li, G. Chen, Y. Zhang, F. Wu, Q. Wang, *J. Am. Chem. Soc.* **2020**, *142*, 14789.

[2] O. T. Bruns, T. S. Bischof, D. K. Harris, D. Franke, Y. Shi, L. Riedemann, A. Bartelt, F. B. Jaworski, J. A. Carr, C. J. Rowlands, M. W. B. Wilson, O. Chen, H. Wei, G. W. Hwang, D. M. Montana, I. Coropceanu, O. B. Achorn, J. Kloepper, J. Heeren, P. T. C. So, D. Fukumura, K. F. Jensen, R. K. Jain, M. G. Bawendi, *Nat Biomed Eng* **2017**, *1*, 0056.

[3] S. Zhu, R. Tian, A. L. Antaris, X. Chen, H. Dai, *Advanced Materials* **2019**, *31*, 1900321.

[4] F. Wang, F. Ren, Z. Ma, L. Qu, R. Gourgues, C. Xu, A. Baghdasaryan, J. Li, I. E. Zadeh, J. W. N. Los, A. Fognini, J. Qin-Dregely, H. Dai, *Nat. Nanotechnol.* **2022**, *17*, 653.

[5] Y. Yang, Y. Xie, F. Zhang, *Advanced Drug Delivery Reviews* **2023**, *193*, 114697.

[6] C. Li, Q. Wang, *ACS Nano* **2018**, *12*, 9654.

[7] E. Hemmer, A. Benayas, F. Légaré, F. Vetrone, *Nanoscale Horiz.* **2016**, *1*, 168.

[8] L. Cognet, C. Leduc, B. Lounis, *Curr. Opin. Chem. Biol.* **2014**, *20*, 78.

[9] H. Shen, L. J. Tauzin, R. Baiyasi, W. Wang, N. Moringo, B. Shuang, C. F. Landes, *Chem. Rev.* **2017**, *117*, 7331.

[10] A. G. Godin, J. A. Varela, Z. Gao, N. Danné, J. P. Dupuis, B. Lounis, L. Groc, L. Cognet, *Nat. Nanotechnol.* **2017**, *12*, 238.

[11] S. Nandi, K. Caicedo, L. Cognet, *Nanomaterials* **2022**, *12*.

[12] N. Fakhri, F. C. MacKintosh, B. Lounis, L. Cognet, M. Pasquali, *Science* **2010**, *330*, 1804.

[13] Y. Chen, D. M. Montana, H. Wei, J. M. Cordero, M. Schneider, X. Le Guével, O. Chen, O. T. Bruns, M. G. Bawendi, *Nano Lett.* **2017**, *17*, 6330.

[14] B. Musnier, K. D. Wegner, C. Comby-Zerbino, V. Trouillet, M. Jourdan, I. Häusler, R. Antoine, J.-L. Coll, U. Resch-Genger, X. Le Guével, *Nanoscale* **2019**, *11*, 12092.

[15] H. Liu, G. Hong, Z. Luo, J. Chen, J. Chang, M. Gong, H. He, J. Yang, X. Yuan, L. Li, X. Mu, J. Wang, W. Mi, J. Luo, J. Xie, X. Zhang, *Advanced Materials* **2019**, *31*, 1901015.

[16] L. Haye, P. I. Diriwari, A. Alhalabi, T. Gallavardin, A. Combes, A. S. Klymchenko, N. Hildebrandt, X. Le Guével, A. Reisch, *Advanced Optical Materials* **2022**, 2201474.

[17] A. Reisch, A. S. Klymchenko, *Small* **2016**, *12*, 1968.

[18] A. H. Ashoka, I. O. Aparin, A. Reisch, A. S. Klymchenko, *Chem. Soc. Rev.* **2023**, DOI 10.1039/D2CS00464J.

[19] Z. Yu, B. Musnier, K. D. Wegner, M. Henry, B. Chovelon, A. Desroches-Castan, A. Fertin, U. Resch-Genger, S. Bailly, J.-L. Coll, Y. Usson, V. Josserand, X. Le Guével, *ACS Nano* **2020**, *14*, 4973.

[20] X. Le Guével, K. D. Wegner, C. Würth, V. A. Baulin, B. Musnier, V. Josserand, U. Resch-Genger, J. Coll, *Chem. Commun.* **2022**, *58*, 2967.

[21] C. J. Martínez Rivas, M. Tarhini, W. Badri, K. Miladi, H. Greige-Gerges, Q. A. Nazari, S. A. Galindo Rodríguez, R. Á. Román, H. Fessi, A. Elaissari, *International Journal of Pharmaceutics* **2017**, *532*, 66.

[22] X. Yan, J. Bernard, F. Ganachaud, *Advances in Colloid and Interface Science* **2021**, *294*, 102474.

[23] T. Chen, Y. Peng, M. Qiu, C. Yi, Z. Xu, *Nanoscale* **2023**, *15*, 3594.

[24] B. Andreiuk, A. Reisch, E. Bernhardt, A. S. Klymchenko, *Chemistry – An Asian Journal* **2019**, *14*, 836.

[25] A. Reisch, D. Heimburger, P. Ernst, A. Runser, P. Didier, D. Dujardin, A. S. Klymchenko, *Advanced Functional Materials* **2018**, *28*, 1805157.

[26] K. Welsher, Z. Liu, S. P. Sherlock, J. T. Robinson, Z. Chen, D. Daranciang, H. Dai, *Nat. Nanotechnol.* **2009**, *4*, 773.
[27] Z. Gao, N. Danné, A. Godin, B. Lounis, L. Cognet, *Nanomaterials* **2017**, *7*, 393.
[28] J. G. Duque, A. N. G. Parra-Vasquez, N. Behabtu, M. J. Green, A. L. Higginbotham, B. K. Price, A. D. Leonard, H. K. Schmidt, B. Lounis, J. M. Tour, S. K. Doorn, L. Cognet, M. Pasquali, *ACS Nano* **2010**, *4*, 3063.
[29] N. Goswami, Q. Yao, Z. Luo, J. Li, T. Chen, J. Xie, *J. Phys. Chem. Lett.* **2016**, *7*, 962.
[30] F. N. Soria, C. Paviolo, E. Doudnikoff, M.-L. Arotcarena, A. Lee, N. Danné, A. K. Mandal, P. Gosset, B. Dehay, L. Groc, L. Cognet, E. Bezard, *Nat. Commun.* **2020**, 1.
[31] C. Paviolo, J. S. Ferreira, A. Lee, D. Hunter, I. Calaresu, S. Nandi, L. Groc, L. Cognet, *Nano Lett.* **2022**, *22*, 6849.
[32] A. Volk, C. J. Kähler, *Exp Fluids* **2018**, *59*, 75.
[33] N.-S. Cheng, *Ind. Eng. Chem. Res.* **2008**, *47*, 3285.
[34] X. Michalet, *Phys. Rev. E* **2010**, *82*, 041914.